ORIGINAL ARTICLE

OPEN ACCESS

Computation Study of Magnetized Darcy-Forchheimer Tangent Hybrid Nanofluid Flow Bounded by Stretchable Surface using Three-Stage Lobatto IIIA Scheme.

Muhammad Umar Farooq [1], Aqib Majeed [2], Farzan Majeed Noori [3]

Authors' Affiliation:

[1]Department of Mathematics, The University of Faisalabad, Punjab, Pakistan
Email: umarfarooq06263@gmail.com

[2]Department of Mathematics, The University of Faisalabad, Punjab, Pakistan
Email: mjaaqib@gmail.com

[3]Postdoctoral Fellow, Department of Informatics, University of Oslo, Norway
Email: farzanmn@ifi.uio.no

Article History:

Submitted: April 06, 2025
Revised: June 19, 2025
Accepted: June 26, 2025
Published online: June 30, 2025

Corresponding author(s):

Muhammad Umar Farooq
Email: umarfarooq06263@gmail.com

ABSTRACT

Current research explores the intricate dynamics of Darcy–Forchheimer flow in a magnetized tangent hyperbolic hybrid nanofluid.$(SiO_2: Al_2O_3/H_2O)$, incorporating the effects of heat and mass transfer, thermal radiation, and a porous medium. Hybrid nanofluids, renowned for their enhanced thermal conductivity and modified rheological behavior, have emerged as transformative materials in energy and industrial applications. The governing nonlinear partial differential equations (PDEs) are reformulated into ordinary differential equations (ODEs) using similarity transformations and solved numerically via a three-stage Lobatto scheme with the help of MATLAB, ensuring computational precision. The study provides a comprehensive analysis of the influence of the Forchheimer number, porosity parameter, magnetic field intensity, and nanoparticle shape factor on flow behavior. Results reveal that increasing the shape factor significantly enhances thermal conductivity, while the Forchheimer effect and porous resistance govern the velocity distribution. A notable observation is that higher values of the Weissenberg number (We), magnetic parameter (M), rotational parameter (λ), and Forchheimer number (Fr) lead to a reduction in velocity boundary layer thickness, whereas the temperature profile exhibits a pronounced increase. Furthermore, the presence of thermal radiation introduces substantial modifications to heat transfer characteristics, optimizing energy transport mechanisms. The findings demonstrate strong alignment with existing literature, reinforcing the robustness of the proposed model. This study offers valuable insights into the complex interplay between magnetohydrodynamics (MHD), porous media, and hybrid nanofluid dynamics, highlighting their potential for next-generation applications in cooling technologies, biomedical systems, and sustainable energy solutions.

Keywords: Darcy-Forchheimer flow, MHD, Porous Space, Thermal radiation, Hybrid nanofluid, Particle shape, Mathematical modeling.

(MSC2020) Codes: 03E72, 03B52, 90B50, 91D30, 03E7

1 | INTRODUCTION

In 1995, [1] introduced the term "Nanofluid." Nanoparticles are suspended in regular base fluids to create the enhanced thermal fluids known as nanofluids. The suspension of different metals, metal oxides, and carbon-based fluids with base liquids such as ethylene glycol, water, oils, etc. Because of their exceptional thermal characteristics, nanoparticles find new uses in a variety of industries. To increase energy efficiency, nanofluids are used in HVAC systems, heat exchangers, and cooling applications in the industrial sector. Nanofluid improves the efficiency of geothermal and solar collector systems in the renewable thermal domain. The MHD flow through the boundary layer of the nanofluid across a stretched sheet was examined by [2]. [3] suggested 3D flow attributed to the stretching surface. [4] Conducted an amazing investigation of the heat transportation mechanism in a nanofluid flow created by an exponentially extending sheet. The numerical results of magnetohydrodynamic flow of nanofluid in the presence of chemical reaction were reported by [5] and [6]. A stretchable geometry's ferromagnetic nano-liquid stream was examined by [7]. [8] described the effects of a magnetic field on the $Al2O3$-water nano-liquid flow and provided an example of the Lorentz force effect on the involved distributions. Magnetohydrodynamics tangent hyperbolic nanofluid flow across an exponentially stretched sheet was investigated numerically by [9].

Two or more distinct nanoparticles are present in the hybrid nanofluid combination, which is distributed within the same base fluid. As a working fluid in convection devices, hybrid nanofluid has recently emerged as the preferred option because of its higher thermal conductivity [10], [11], [12], [13] compared to nanofluid. The thin-film flow of the hybrid nanofluid based on $H2O$-based carbon nanotubes was examined by [14]. The MHD flow of the Cu-$Fe3O4$ / $H2O$ hybrid nanofluid was studied by [15]. The enhanced thermal efficiency of a hybrid nanofluid made of graphene oxide and silver/kerosene oil over a stretched sheet was investigated by [16]. The impacts of tangent hyperbolic hybrid nanofluid on a porous medium, convective slip-boundary constraints, and slip-resistant dissipation on the heat source are comprehensively investigated by [17]. [18] performed heat transfer enhancement in a tangent hyperbolic fluid towards a stretchy surface under the influence of an inclined magnetic field. Similarly, [19] conducted a numerical study on time-dependent tangent hyperbolic hybrid nanofluid flow over a progressively stretching surface. [20] examined stagnation point flow of hyperbolic hybrid nanofluid over a stretching sheet. Under velocity and thermal slip conditions with different base fluids, the proposed work investigates the 2D tangent hyperbolic hybrid nanofluid flow towards a porous stretching sheet with an inclined uniform magnetic field. Solid nanoparticles of copper and aluminum oxide are utilized. At the same time, as base fluids are water and (50% water) + (50% EG mixture) are utilized [21], [22].

Magnetohydrodynamics is used in boundary layer flow to control fluid flow by connecting the magnetic field with fluid flow. Magnetohydrodynamic flow has been widely studied in the past. The study of the magnetic characteristics and behavior of electro-conductive fluids in a magnetic field is known as magnetohydrodynamic flow. Variable viscosity influences on time-dependent MHD nanofluid flow across a stretched surface have been investigated by [23]. [24] examined the effects of boundary layer flow and heat transfer of nanofluid in the presence of a heat source. [25] discussed about time-dependent MHD Casson nanofluid flow with a heat source and radiation. The theoretical studies about the tangent hyperbolic hybrid nanofluid MHD radiative flow with convective conditions across the stretching sheet were analyzed by [26]. The comparative study of MHD tangent hyperbolic hybrid nanofluid flow over a porous stretched sheet with various base fluids was investigated by [27].

The author observed no investigation on the three-dimensional magnetized Darcy-Forchheimer rotating tangent hyperbolic hybrid nanofluid flow over a porous stretching sheet with the effect of thermal radiation. The flow problem consists of system PDEs. These PDEs are changed into system ODEs with the help of a transformation variable. The numerically solved ODEs via the bvp4c package are built in MATLAB software. Our research novelties are: (i) MHD tangent hyperbolic hybrid nanofluid.(SiO_2: Al_2O_3/H_2O) (ii) Darcy-Forchheimer flow, (iii) how radiation parameter, shape factor of nanoparticles and mass flux parameter effect on the rate of transfer (iv) how Brownian motion and thermophoresis parameter impact on rate of mass transfer and motile microorganism number on flow of fluid (v) hybrid nanofluid(SiO_2: Al_2O_3/H_2O) flow and nanofluid(SiO_2/H_2O) flow outcomes are compared.

1.1 | Mathematical Formulation.

Let us consider an incompressible magnetized Darcy-Forchheimer rotating tangent hyperbolic hybrid nanofluid flow across the three-dimensional stretching sheet containing $SiO_2$and Al_20_3 nanoparticles and microorganism. A chosen in such a way stretching along $x - axis$ with fluid velocity. $U_w = a.x$ in a cartesian coordinate system(x, y, z). A uniform strength of a magnetic field $(B_o)$is applied perpendicular to the direction of fluid flow shown in **Fig. 1.** The thermophoresis and Brownian phenomenon in the concentration equation. The temperature, temperature of the wall, and temperature of the free stream are denoted as T, T_w and T_∞ respectively. Also, the concentration of the wall, the concentration, and the free stream concentration are described asC_w, C and C_∞. Similarly, N_∞, N_w and N are defined as free stream motile micro-organism, motile micro-organism of wall, and motile micro-organism respectively. Joule heating effect, velocity slip, or thermal jump, and viscous dissipation are not considered. The leading equations are considered based on the above assumptions and Tiwari and Das [28], [29], [30], [31], [32].

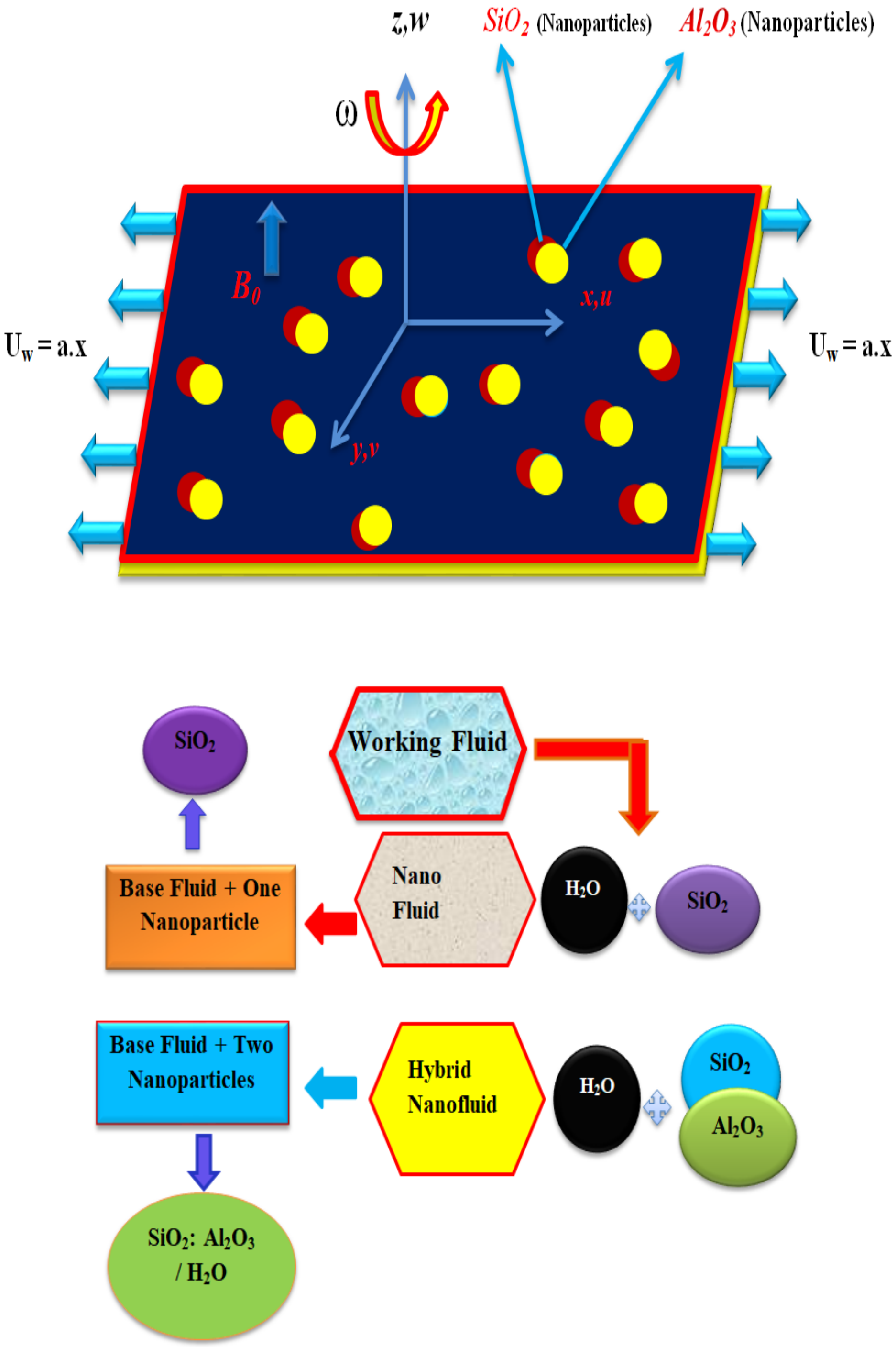

Figure 1. Schematic diagram of the flow problem, working fluid.

Equation of Continuity:

$$\frac{\partial u}{\partial x} + \frac{\partial v}{\partial y} + \frac{\partial w}{\partial z} = 0, \qquad (1)$$

Equation of Momentum in x-direction:

$$\rho_{hnf}\left(u\frac{\partial u}{\partial x} + v\frac{\partial u}{\partial y} + w\frac{\partial u}{\partial z} - 2\Omega v\right) = \mu_{hnf}\left((1-n) + \sqrt{2}n\Gamma\frac{\partial u}{\partial z}\right)\frac{\partial^2 u}{\partial z^2} - \sigma B_0^2 u - Fu^2 -$$

$$\frac{\mu_{hnf}}{K^*}u, \tag{2}$$

Equation of Momentum in y-direction:

$$\rho_{hnf}\left(u\frac{\partial v}{\partial x} + v\frac{\partial v}{\partial y} + w\frac{\partial v}{\partial z} - 2\Omega u\right) = \mu_{hnf}\left((1-n) + \sqrt{2}n\Gamma\frac{\partial v}{\partial z}\right)\frac{\partial^2 v}{\partial z^2} - \sigma B_0^2 v - Fv^2 - \frac{\mu_{hnf}}{K^*}v, \tag{3}$$

Equation of Energy:

$$u\frac{\partial T}{\partial x} + v\frac{\partial T}{\partial y} + w\frac{\partial T}{\partial z} = \mu_{hnf}\frac{\partial^2 T}{\partial z^2} - \frac{1}{(\rho C_p)_{hnf}} - \frac{16\sigma^* T_\infty^3}{3k^*}\frac{\partial^2 T}{\partial z^2} \tag{4}$$

Concentration Equation:

$$u\frac{\partial C}{\partial x} + v\frac{\partial C}{\partial y} + w\frac{\partial C}{\partial z} = D_B\frac{\partial^2 C}{\partial z^2} + \frac{D_B}{T_\infty}\frac{\partial^2 T}{\partial z^2} \tag{5}$$

Motile Microorganism Equation:

$$u\frac{\partial N}{\partial x} + v\frac{\partial N}{\partial y} + w\frac{\partial N}{\partial z} + \frac{bW_c}{C_w - C_\infty}\left[\frac{\partial}{\partial z}\left(N\frac{\partial C}{\partial z}\right)\right] = D_m\frac{\partial^2 N}{\partial z^2} \tag{6}$$

With boundary [33]:

$$\mathrm{u} = U_{\mathrm{w}}L \ ,\mathrm{v} = 0, w = 0,\ C = C_w,\quad N = N_w, T = T_{\mathrm{w}} \qquad \text{at } z = 0$$
$$\mathrm{u} \to 0, \mathrm{v} \to 0, \mathrm{w} \to 0, T \to T_\infty, C \to C_\infty, N \to N_\infty, \qquad \text{at } z \to \infty$$

Table 2. Thermophysical properties of nano and hybrid nanoparticles [34].

Thermophysical characteristics	**Nanofluids(SiO_2/H_2O)**	**Hybrid Nanofluids (Zn-TiO_2: H_2O)**
Density (ρ), kg/m^3	$\rho_{\mathrm{nf}} = \phi_2\rho_{\mathrm{s}} + (1-\phi_2)\rho_{\mathrm{f}}$	$\rho_{\mathrm{hnf}} = \phi_2\rho_{\mathrm{s2}} + \{(1-\phi_1)\rho_{\mathrm{f}} + \phi_1\rho_{\mathrm{s1}}\}(1-\phi_2)$
Heat capacity (C_p), J/K	$(\rho C_p)_{\mathrm{nf}} = \phi_2(\rho C_p)_{\mathrm{s}} + (\rho C_p)_{\mathrm{f}}(1-\phi_2)$	$(\rho C_p)_{\mathrm{hnf}} = \phi_2(\rho C_p)_{\mathrm{s2}} + (1-\phi_2)\{\phi_1(\rho C_p)_{\mathrm{s1}} + (\rho C_p)_f(1-\phi_1)$
Viscosity ((μ)), N·s/m^2	$\mu_{\mathrm{nf}} = \mu_{\mathrm{f}}(1-\phi_2)^{-2.5}$	$\mu_{\mathrm{hnf}} = \mu_{\mathrm{f}}(1-\phi_1)^{-2.5}(1-\phi_2)^{-2.5}$

Thermal conductivity (k_f), W/m·K	$\frac{k_{nf}}{k_f}=\frac{k_s+k_f(n-1)-\phi_2(n-1)(k_f-k_s)}{k_s+k_f(n-1)+(k_f-k_s)\phi_2}$	$\frac{k_{bf}}{k_f}=\frac{k_{s1}+(n-1)k_f-(n-1)(k_f-k_{s1})\phi_1}{k_{s1}+(n-1)k_f+(k_f-k_{s1})\phi_1}$ $\frac{k_{hnf}}{k_{bf}}=\frac{k_{s2}-\phi_2(n-1)(k_{bf}-k_{s2})+k_{bf}(n-1)}{k_{s2}+(n-1)k_{bf}+(k_{bf}-k_{s2})\phi_2}$

The appropriate scaling variables are:

$$u = axf'(\eta), \quad v = axg(\eta), \quad w = -\sqrt{av_f}f(\eta),$$
$$\eta = (\frac{a}{v_f})^{0.5}z, \ \Phi(\eta) = \frac{C-C_\infty}{C_w-C_\infty}, \theta(\eta) = \frac{T-T_\infty}{T_f-T_\infty}, \ \frac{N-N_\infty}{N_w-N_\infty} = \chi(\eta). \tag{8}$$

Using the similarity approach, the non-dimensional form of Eqs. (2-6) are as follows:

$$((1-n)+nWef'')\,f''' + B_1B_2\left(ff''-f'^2+2\lambda g\right) - B_1Mf' - B_1Frf'^2 - P_of' = 0, \tag{9}$$

$$((1-n)+nWeg')\,g'' + B_1B_2(fg'-f'g-2\lambda f') - B_1Mg - B_1Frg^2 - P_og = 0, \tag{10}$$

$$\frac{1}{B_3}\left(B_4+\frac{4}{3}Rd\right)\theta'' + Prf\theta' = 0, \tag{11}$$

$$\Phi'' + \theta''\frac{Nt}{Nb} + \Phi'Le = 0, \tag{12}$$

$$\chi'' + Lbf\chi' - [\chi'\Phi' + (\chi+\delta_1)\Phi'']Pe = 0, \tag{13}$$

Subject to boundary constraints are:

$$\begin{gathered} f(0)=S, \quad f'(0)=L, \quad \chi(0)=1 \quad \theta(0)=1, \Phi(0)=1 \quad g(0)=0, \\ \theta(\eta)\to 0, \quad \Phi(\infty)\to 0, \quad g(\eta)\to 0, \quad f'(\eta)\to 0, \chi(\infty)\to 0 \quad \text{at } \eta\to\infty \end{gathered} \tag{14}$$

Dimensionless quantities are as follows:

Name of Parameter	**Notations**	**Values**
Weissenberg number	We	$We\frac{\sqrt{2a}\Gamma ax}{\sqrt{v_f}}$
Magnetic parameter	M	$M=\frac{\sigma B_0^2}{a\rho_f}$
Prandtl number	Pr	$Pr=\frac{\kappa_{bf}}{v_f(\rho C_p)_f}$
Rotational parameter	λ	$\lambda=\frac{\Omega}{a}$
Inertia Coefficient	Fr	$Fr=\frac{C_b}{\rho_f\,k^{*\frac{1}{2}}}$
Radiation parameter	Rd	$Rd=\frac{4\sigma T_\infty^3}{k^*\kappa_{bf}}$

Porosity parameter	Po	$Po = \frac{\nu_f}{ak^*}$
Local Reynolds number	Re_x	$Re_x = \frac{u_w x}{\nu_f}$
Brownian motion	Nb	$\frac{\tau D_B(C_w - C_\infty)}{\nu_f}$
Thermophoresis parameter	Nt	$\frac{\tau D_T(T_w - T_\infty)}{T_\infty \nu_f}$
Lewis number	Le	$\frac{\nu_f}{D_B}$
Peclet number	Pe	$\frac{bW_c}{D_m}$
Microorganism concentration difference parameter	δ_1	$\frac{N_\infty}{N_w - N_\infty}$
Bioconvection Lewis number	Lb	$\frac{\nu_f}{D_m}$

Also,

$$B_1 = (1-\phi_1)^{5/2}(1-\phi_2)^{5/2},$$

$$B_2 = \left\{(1-\phi_1) + \phi_1 \frac{\rho_{s1}}{\rho_f}\right\}(1-\phi_2) + \frac{\rho_{s2}}{\rho_f}\phi_2,$$

$$B_3 = \left\{(1-\phi_1) + \phi_1 \frac{(\rho C_p)_{s1}}{(\rho C_p)_f}\right\}(1-\phi_2) + \phi_2 \frac{(\rho C_p)_{s2}}{(\rho C_p)_f},$$

$$B_4 = \frac{k_{\mathrm{hnf}}}{k_{\mathrm{bf}}}.$$

Skin friction coefficient (C_{fx}) and (C_{fy}), motile number(Nn_x), Sherwood number $(Sh_r)$and Nusselt number (Nu_x) respectively. These quantities are described are follows:

$$C_{fx} = \mu_{hnf}\left((1-n) + \sqrt{2}n\Gamma \frac{\partial u}{\partial z}) \frac{\partial^2 u}{\partial z^2}\right)|_{z=0},$$

$$C_{fy} = \mu_{hnf} \frac{\partial v}{\partial z}|_{z=0},$$

$$Nu_x = -\frac{x k_{hnf}}{k_f(T_w - T_\infty)}[(\frac{\partial T}{\partial z})_{z=0} - q_r|_{z=0}].$$

$$Sh_x = -\frac{x\, k_{hnf}}{k_f(C_w - C_\infty)} \frac{\partial C}{\partial z}|_{z=0},$$

$$Nn_x = -\frac{x k_{hnf}}{k_f(N_w - N_\infty)} D_m \frac{\partial N}{\partial z}|_{z=0}, \tag{15}$$

Using equations (8) and (15), we get

$$Re_x^{0.5}Cf_x = \frac{1}{B_1}\left(1-n+\frac{n}{2}Wef''(0)\right)f''(0),$$

$$Re_x^{0.5}Cf_y = \frac{1}{B_1}\left(1-n+\frac{n}{2}Weg'(0)\right)g'(0)\,,$$

$$\mathrm{Re}_x^{-0.5}Nu_x = -\left(B_4+\frac{4}{3}Rd\right)\theta'(0), \tag{16}$$

$$Re_x^{-0.5}Sh_r = -\Phi'(0),$$

$$Re_x^{-0.5}Nn_x = -\chi'(0).$$

In which $Re_x = \frac{u_w x}{\nu_f}$ represents the local Reynolds number.

3| METHODS AND SOLUTIONS

The non-linear ordinary differential equations (9-13) for velocity profile, temperature field, concentration distribution, and motile microbes, along with boundary relation (14), are solved by utilizing MATLAB computational software process can be seen in Fig.2. For this procedure, we change first convert them into first-order reduction of the above DEs, which are as follows:

$$f' = z_2, f = z_1, f'' = z_3, f''' = zz_1, g = z_4, g' = z_5, g'' = zz_2, \theta = z_6,$$

$$\theta' = z_7, \theta'' = zz_3, \phi = z_8, \phi' = z_9, \phi'' = zz_4, \chi = z_{10}, \chi' = z_{11}, \chi'' = zz_5,$$

$$zz_1 = \left(\frac{-1}{((1-n)+nWez_3)}\right)(B_1\,B_2(z_1z_3 - {z_2}^2 + 2\lambda z_4) - B_1Mz_2 - B_1Fr{z_2}^2 - Poz_2),$$

$$zz_2 = \left(\frac{-1}{((1-n)+nWez_5)}\right)(B_1\,B_2(z_1z_5 - z_2z_4 - 2\lambda z_2) - B_1Mz_4 - B_1Fr{z_4}^2 - Poz_4),$$

$$zz_3 = -P_rB_3(-1/(B_4+(4/3)Rd))z_1z_7,$$

$$zz_4 = Le(z_1z_8 + \sigma\exp\left(-\frac{E}{1+\psi z_6}\right)(1+\psi z_6)z_8,$$

$$zz_5 = [(\delta_1 + Z_{10})zz_4 + z_9z_{11}]Pe - Lb\, z_1z_{11},$$

Subjected to boundary conditions:

$$z_2 = L\ , z_1 = S\ , z_4 = 0\ , z_6 = 1, z_8 = 1, z_{10} = 1\ as\eta = 0,$$

$$z_6 = 0, z_4 = 0, z_2 = 0\ , z_{10} = 0, z_8 = 0\ \ as\eta \to \infty. \tag{17}$$

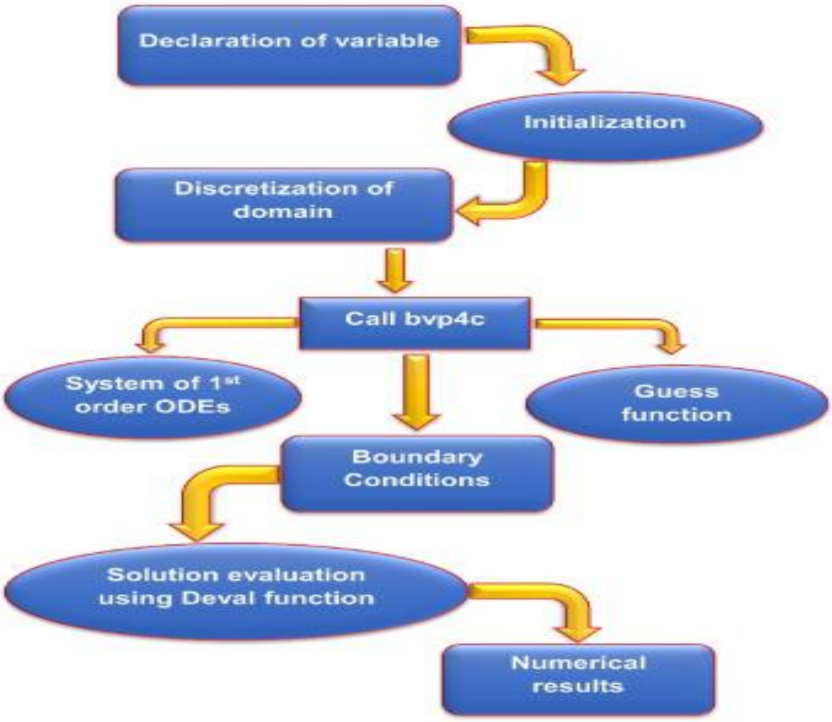

Figure 2. Algorithm of numerical scheme

4 | RESULTS AND DISCUSSION

In this section, numerical outcomes for the three-dimensional magnetized hyperbolic tangent hybrid nanofluid Darcy-Forchheimer flow over the stretching sheet are presented. For motile micro-organism concentration, velocity, and Temperature profiles. The influence dimensionless parameters like as magnetic parameter(M), Wissenberg number(We), porosity parameter(Po), rotational parameter(λ), mass flux parameter(S), Darcy-Forchheimer number (Fr), thermophoretic parameter(Nt), Brownian motion parameter(Nb), Lewis number(Le), biconvection Lewis number(Lb) and Plect number (Pe)has been investigated. The non-linear system of differential equations is solved via bvp4c is built in MATLAB, to get numerical outcomes of the converted system of differential equations. In Table 3, we described the outcomes for $f'(0)$ and $g(0)$ for the various values of $\boldsymbol{Pr}$ while the other values of parameters are fixed. These outcomes are reliable, as compared to the outcomes with previous published studies [34],[35].

Figures 2(a-n) present the effect of$n, We, M, \lambda, P_o, Fr$ and S on the velocity of fluid components $f'(\eta)$and $g(\eta)$. Figs. 2(a-b) indicate that n illustrates the condensed behavior of the fluid velocity. The n is directly proportional to the resistance of the fluid rate under discussion. It is observed that fluid resistance rises as boost$n$the $f'(\eta)$ but$g(\eta)$ upgrade. Table 4 shows the friction factor for HNF. $(SiO_2{:}\, Al_2O_3/H_2O)$and NF$(SiO_2/H_2O)$ along $(\boldsymbol{Re_x^{0.5}Cf_x})$isreducing and$(\boldsymbol{Re_x^{0.5}Cf_y})$ rise with high values of n.$We$is defined as the ratio between the scale of fluid flow time relaxation time. From Figs. 2(c-d) it is seen that when Werises the $f'(\eta)$fall down and $g(\eta)$is increasing because the fluid flow for further time required. Table 4 signifies the friction factor of HNF.($SiO_2: Al_2O_3/H_2O$)and NF (SiO_2/H_2O) along ($\boldsymbol{Re_x^{0.5}Cf_x}$)and($\boldsymbol{Re_x^{0.5}Cf_y}$)are reducing with high values of We.The influence of Mon $f'(\eta)$ and $g(\eta)$are displayed in Figs. 2(e-f). Higher M, $f'(\eta)$decreases and $g(\eta)$ Increases (see in Figs. 2(e-f)). The physical points of view decrease the fluid velocity due to the resistive force known as the Lorentz force. When M rises, the Lorentz force boost, therefore,$f'(\eta)$ decrease and $g(\eta)$ Increase. Table 4 examined the friction factor of HNF($SiO_2: Al_2O_3/H_2O$)and NF(SiO_2/H_2O) along ($\boldsymbol{Re_x^{0.5}Cf_x}$)isreducing and($\boldsymbol{Re_x^{0.5}Cf_y}$) rise with high values of M.

The effect on the $f'(\eta)$ and $g(\eta)$ of $\lambda$are recorded in Figs. 2(g-h). When variation in λ, then $f'(\eta)$ Show negative behavior and $g(\eta)$ Show positive behavior. Table 4 illustrates the friction factor of HNF($SiO_2: Al_2O_3/H_2O$) and NF(SiO_2/H_2O) along ($\boldsymbol{Re_x^{0.5}Cf_x}$)and($\boldsymbol{Re_x^{0.5}Cf_y}$)reduces for higher values of λ. From the viewpoint of physically, the reason is that the involved Goriolis forces are (-$2\lambda f'$) and ($2\lambda g$) in equations (9& 10). When grow the values of λ the rise, the Goriolis forces in the boundary layer rise. Reducing the fluid velocity due to the λ results in heat transfer being low near the surface, causing to increase in the local temperature. The decrease the convection and mixing near to surface leads to greater gradients of concentration near the sheet. Figures 2 (i-j) show the influence of P_o on $f'(\eta)$ and $g(\eta)$. Greater values ofP_o, the $f'(\eta)$fall down and $g(\eta)$ boost (see in Figures 2 (i-j)). Table 4 reveals the friction factor of HNF($SiO_2: Al_2O_3/H_2O$)and NF(SiO_2/H_2O) along ($\boldsymbol{Re_x^{0.5}Cf_x}$)isreducing and($\boldsymbol{Re_x^{0.5}Cf_y}$) rise with high values of Po. Physically, the porosity parameter values are larger than the velocity, and the thickness boundary layer of momentum are both decreased. The contact surface of liquid and the surface of solid effects the properties of flow, and the increase in this is due to the presence of a porous medium. Influence of Fr on the $f'(\eta)$ and $g(\eta)$are shown in Fig 2(k-l). Physically, the reason is that fluid motion due to the resistance of the primary profile of velocity distributions has declined proportionally to the Darcy-Forchheimer number.

Table 4 indicates the friction factor of HNF ($SiO_2: Al_2O_3/H_2O$) and NF (SiO_2/H_2O) along ($\boldsymbol{Re_x^{0.5}Cf_x}$)isreducing and($\boldsymbol{Re_x^{0.5}Cf_y}$) rise with high values of Fr. The higher values of Fr than the curves of $f'(\eta)$ Reducing and curves of g(n) rise see in fig 2 (k-l). Figs. 2(m-n) shows the impact of Son $f'(\eta)$and $g(\eta)$ As the values of s boost, they reduce. $f'(\eta)$and upgrade $g(\eta)$Physically, the mass flux parameter removes the fluid from the boundary layer, thinner boundary layer. This increases the gradient of fluid velocity near the surface, boosts the shear stress, and decreases the x −component of fluid velocity and grows the x −component of fluid velocity. Table 4 states that the friction factor of HNF($SiO_2: Al_2O_3/H_2O$)and NF(SiO_2/H_2O) along ($\boldsymbol{Re_x^{0.5}Cf_x}$)isreducing and($\boldsymbol{Re_x^{0.5}Cf_y}$) rise with high values of S.Figs. 3(a-g) illustrate the influence on $\theta(\eta)$ of $n, We, M, \lambda, Fr,\ S, Rd$, and q. As n increases, then $\theta(\eta)$ grow as shown in Fig. 3(a). Table 5 signifies that Nusselt number ($\boldsymbol{Re_x^{-0.5}Nu_x}$)for HNF($SiO_2: Al_2O_3/H_2O$)and NF($SiO_2/H_2O$)reduce with high values of n. The effect of We on $\theta(\eta)$ is shown in Fig. 3(b). As the result greater the values of We, the $\theta(\eta)$Increase. From Table 5, seen that the Nusselt number ($\boldsymbol{Re_x^{-0.5}Nu_x}$)for hybrid nanofluid($SiO_2$: Al_2O_3/H_2O)and nanofluid(SiO_2/H_2O)reduce with large values of We.We is defined as the ratio between the scale of fluid flow time relaxation time. The influence of values of M, impact on $\theta(\eta)$illustrate in Fig. 3(c). The rises values of M, impact on $\theta(\eta)$ boost (See in Fig. 3(c)).From Table 5, seen that the Nusselt number ($\boldsymbol{Re_x^{-0.5}Nu_x}$)for hybrid nanofluid($SiO_2$: Al_2O_3/H_2O) and nanofluid(SiO_2/H_2O)reduce with large values of M. The physical points of view that reduce the thickness of the boundary layer due to the resistive force Lorentz force. Fig. 3(d) displays the impact on $\theta(\eta)$ of λ. The boost values ofλ, $\theta(\eta)$ upgrade smoothly.

The heat transfer rate is faster in the hybrid nanofluid.(SiO_2: Al_2O_3/H_2O)as compared to nanofluid(SiO_2/H_2O). Table 5 shows that the Nusselt number ($Re_x^{-0.5}Nu_x$)for HNF(SiO_2: Al_2O_3/H_2O) and NF(SiO_2/H_2O)reduce with large values of λ. Fig. 3(e) epitomizes the effect on $\theta(\eta)$ of Fr.The boost values ofFr, $\theta(\eta)$ rise smoothly. The heat transfer rate is faster in the hybrid nanofluid.(SiO_2: Al_2O_3/H_2O) as compared to nanofluid(SiO_2/H_2O). Table 5 illustrates that Nusselt number ($Re_x^{-0.5}Nu_x$)for hybrid nanofluid(SiO_2: Al_2O_3/H_2O)and nanofluid(SiO_2/H_2O)reduce with large values of Fr. Fig. 3(f) illustrates the effect on $\theta(\eta)$ of S. The boost values of$S$, $\theta(\eta)$ rise smoothly. The rate of heat transfer is faster in HNF(SiO_2: Al_2O_3/H_2O) as associated with NF(SiO_2/H_2O). From Table 5, seen that the Nusselt number ($Re_x^{-0.5}Nu_x$)for hybrid nanofluid(SiO_2: Al_2O_3/H_2O) and nanofluid(SiO_2/H_2O) grow with large values of S. Figure 3(g) display the impact on $\theta(\eta)$ of Rd. The boost values of Rd, $\theta(\eta)$ upgrade smoothly. The heat transfer rate is faster in the hybrid nanofluid.(SiO_2: Al_2O_3/H_2O) as compared to nanofluid(SiO_2/H_2O). From Table 5, seen that the Nusselt number ($Re_x^{-0.5}Nu_x$)for hybrid nanofluid(SiO_2: Al_2O_3/H_2O)and nanofluid(SiO_2/H_2O)reduce with high values of Rd.

The radiation parameter illustrates how thermal radiation contributes to heat transport in terms of physics. Therefore, the temperature of the boundary layer increases as the radiation parameter increases. Fig. 3(h) shows how the shape factor (n) affects the hybrid nanofluid's heat transfer rate performance. (SiO_2: Al_2O_3/H_2O). When nanoparticles are shaped like blades, the rate of heat transmission is highest; when they are shaped like spheres, the rate of heat transfer is lowest. From a physical perspective, Blade's thermal conductivity is higher than that of platelets, which are spherical and cylindrical in form. Consequently, the rate of transfer is higher than that of platelets, spherical, and cylindrical nanoparticles. Consequently, the rate of transfer is higher than that of platelets, spherical, and cylindrical nanoparticles. Table 5 shows that for both hybrid nanofluids(SiO_2: Al_2O_3/H_2O) and nanofluids (SiO_2/H_2O), the Nusselt number ($\boldsymbol{Re_x^{-0.5}Nu_x}$) increases with increasing values of q.

The influence on$\phi(\eta)$ against various physical parameters are including $Nt, Nb$and Lb displayed in Figures 4(a-c). The consequences of Nt and Nbon the $\phi(\eta)$as shown in Figs. 4(a-b). The enhancement in Ntboost the $\phi(\eta)$ curves (See in Fig 4(a)). The enhancement in Nbreduce the $\phi(\eta)$ curves (see in Figure 4(b)). Nt Changes the concentration profile by causing particles to migrate towards regions with higher or lower temperature gradients, depending on their properties. In regions with a strong temperature gradient, particles undergoing positive Nt tend to migrate towards colder regions, increasing particle concentrations in those areas. The distribution of concentration may become non-uniform as a result of the combined impacts of Nt and additional transport mechanisms, such as diffusion, advection, and sedimentation. Fig 4(c) illustrates the effect of Lb on$\phi(\eta)$. It is observed that rise the variation in Lb, the influence continuously boosts (see in Fig 4(c)). Physical point of view, the Lewis number is the heat transfer constraint for nanofluid and hybrid nanofluid. Greater Lewis number values have less of an effect on the volume fraction of nanoparticles. Le has an inverse relationship with the boundary's thickness.

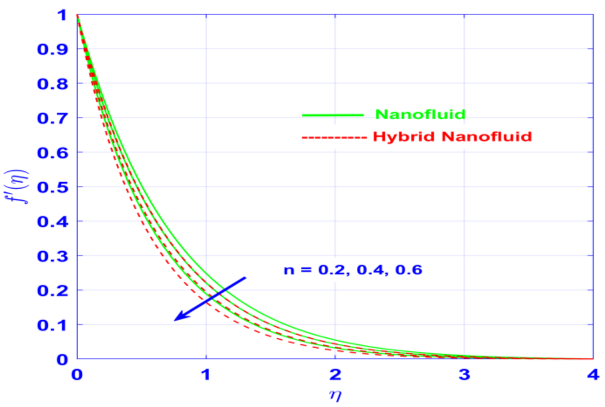

(a)

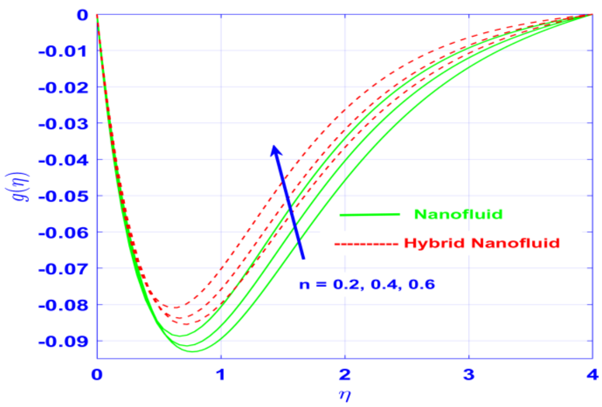

(b)

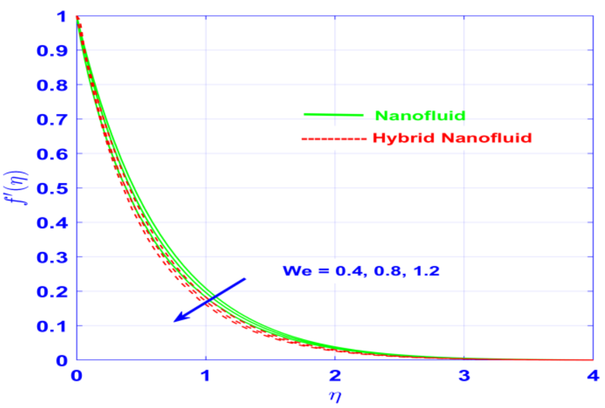

(c)

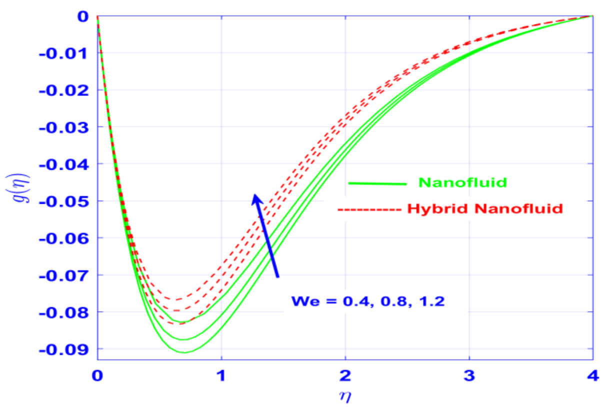

(d)

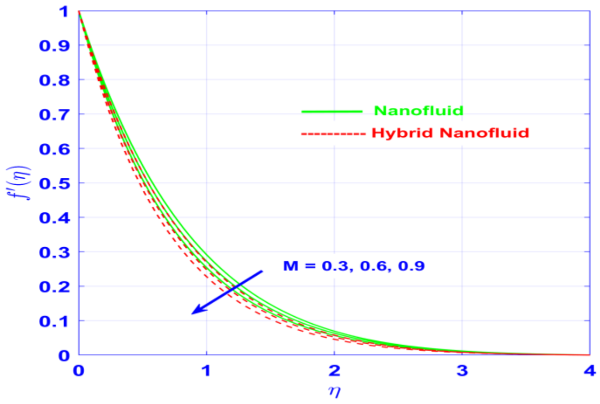

Nanofluid
Hybrid Nanofluid
M = 0.3, 0.6, 0.9
$f'(\eta)$
η

(e)

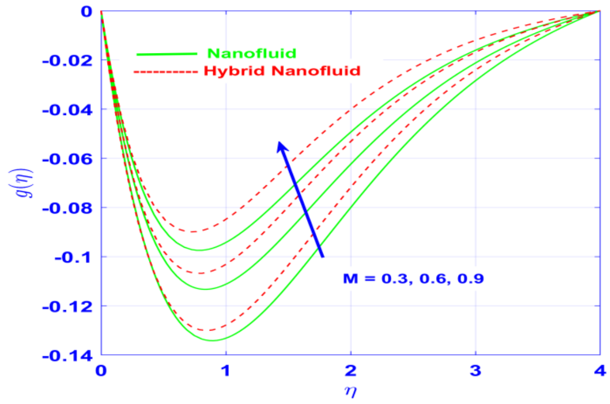

Nanofluid
Hybrid Nanofluid
M = 0.3, 0.6, 0.9
$g(\eta)$
η

(f)

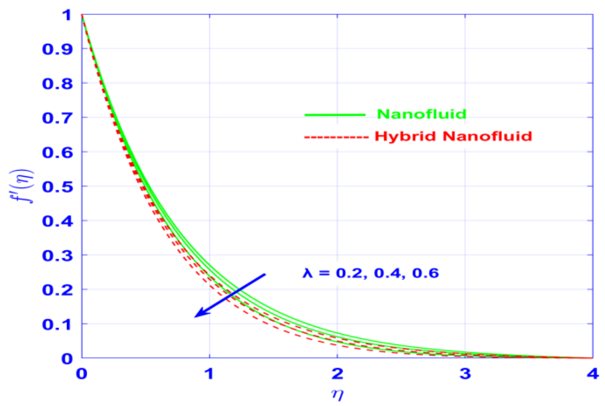

Nanofluid
Hybrid Nanofluid
λ = 0.2, 0.4, 0.6
$f'(\eta)$
η

(g)

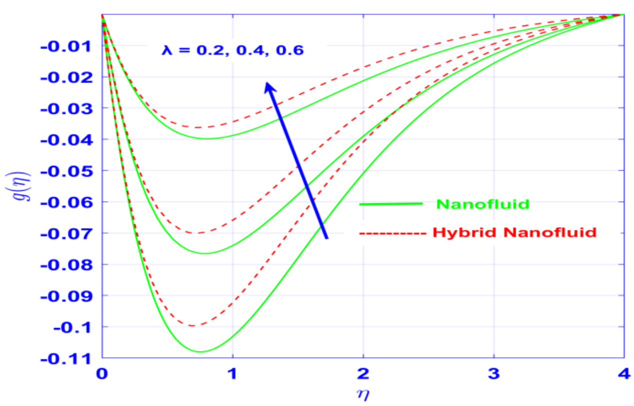

λ = 0.2, 0.4, 0.6
Nanofluid
Hybrid Nanofluid
$g(\eta)$
η

(h)

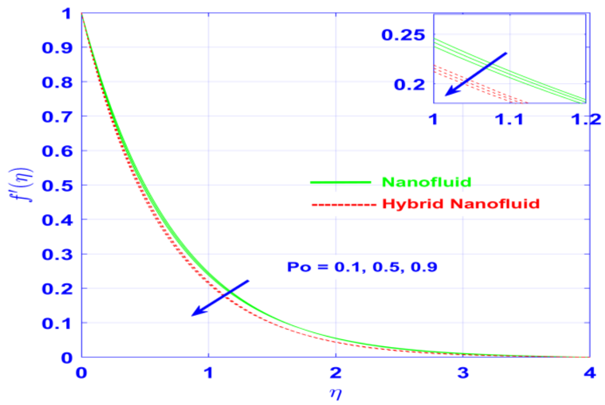

Nanofluid
Hybrid Nanofluid
Po = 0.1, 0.5, 0.9
$f'(\eta)$
η

(i)

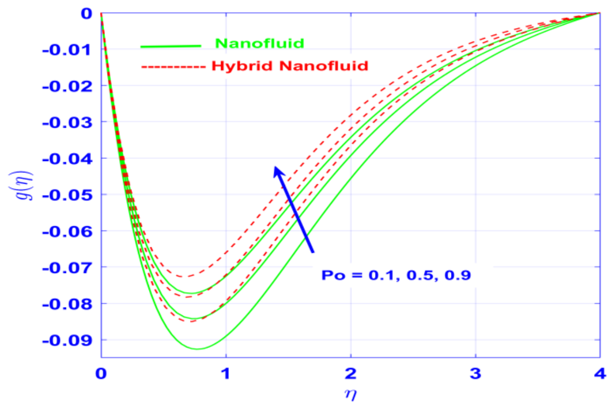

Nanofluid
Hybrid Nanofluid
Po = 0.1, 0.5, 0.9
$g(\eta)$
η

(j)

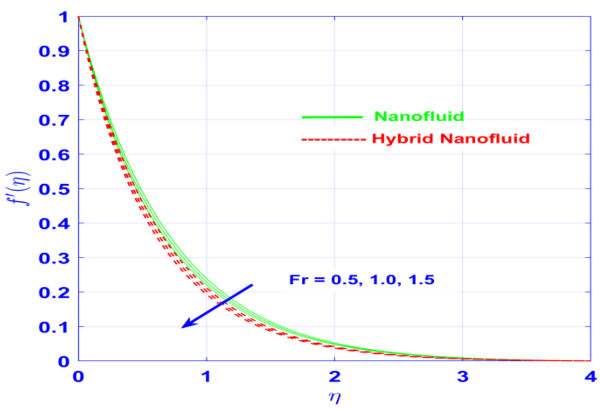

Nanofluid
Hybrid Nanofluid
Fr = 0.5, 1.0, 1.5
$f'(\eta)$
η

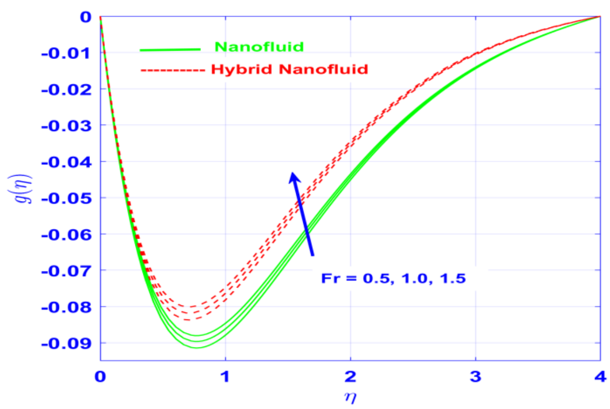

Nanofluid
Hybrid Nanofluid
Fr = 0.5, 1.0, 1.5
$g(\eta)$
η

(k) (l)

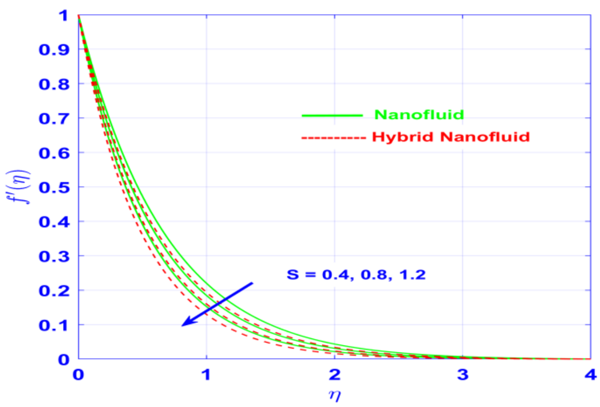

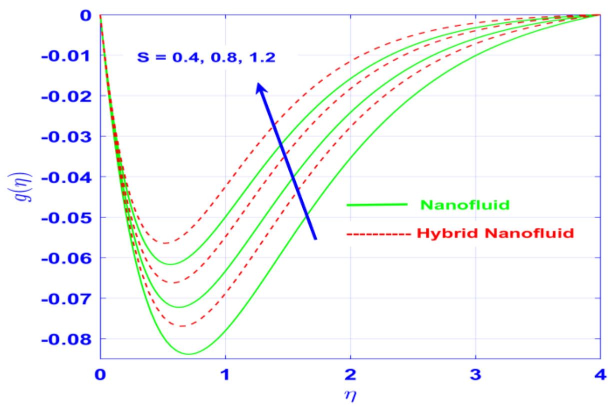

(m) (n)

Figure 3(a-n). Effect of $n, We, M, \lambda, Po, Fr$, and S on $f'(\eta)$ and $g(\eta)$.

/

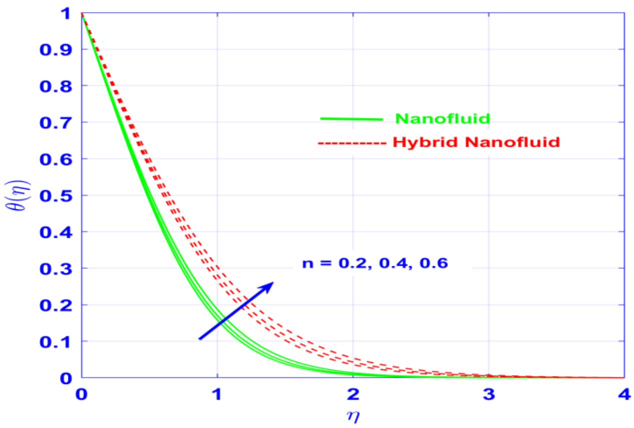

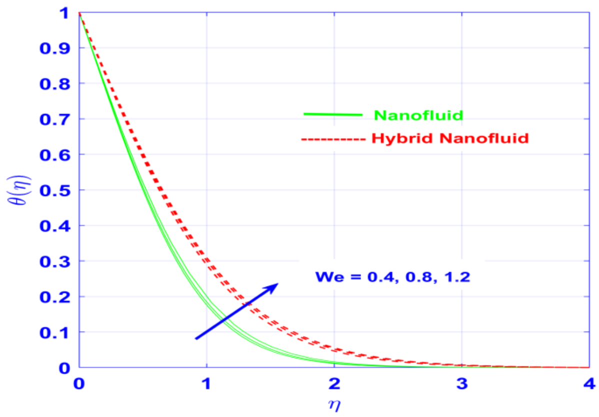

(a) (b)

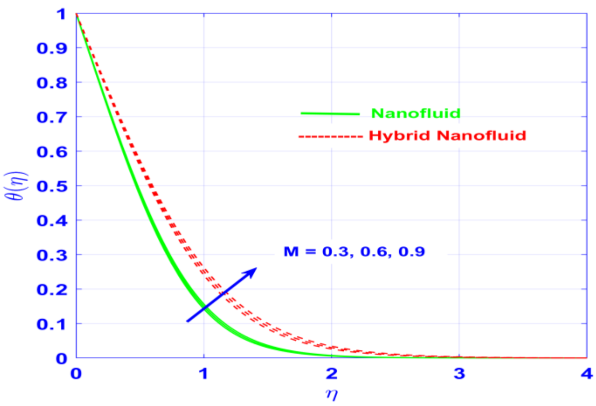

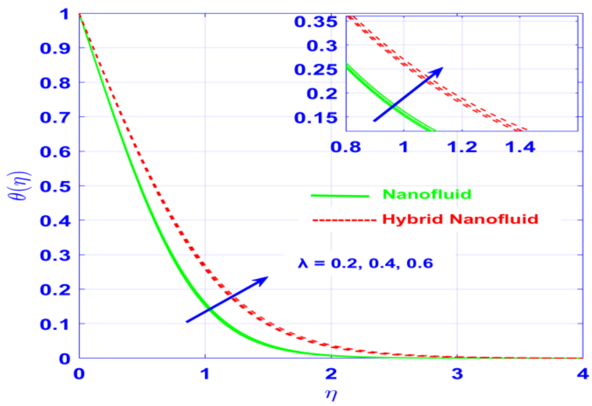

(c) (d)

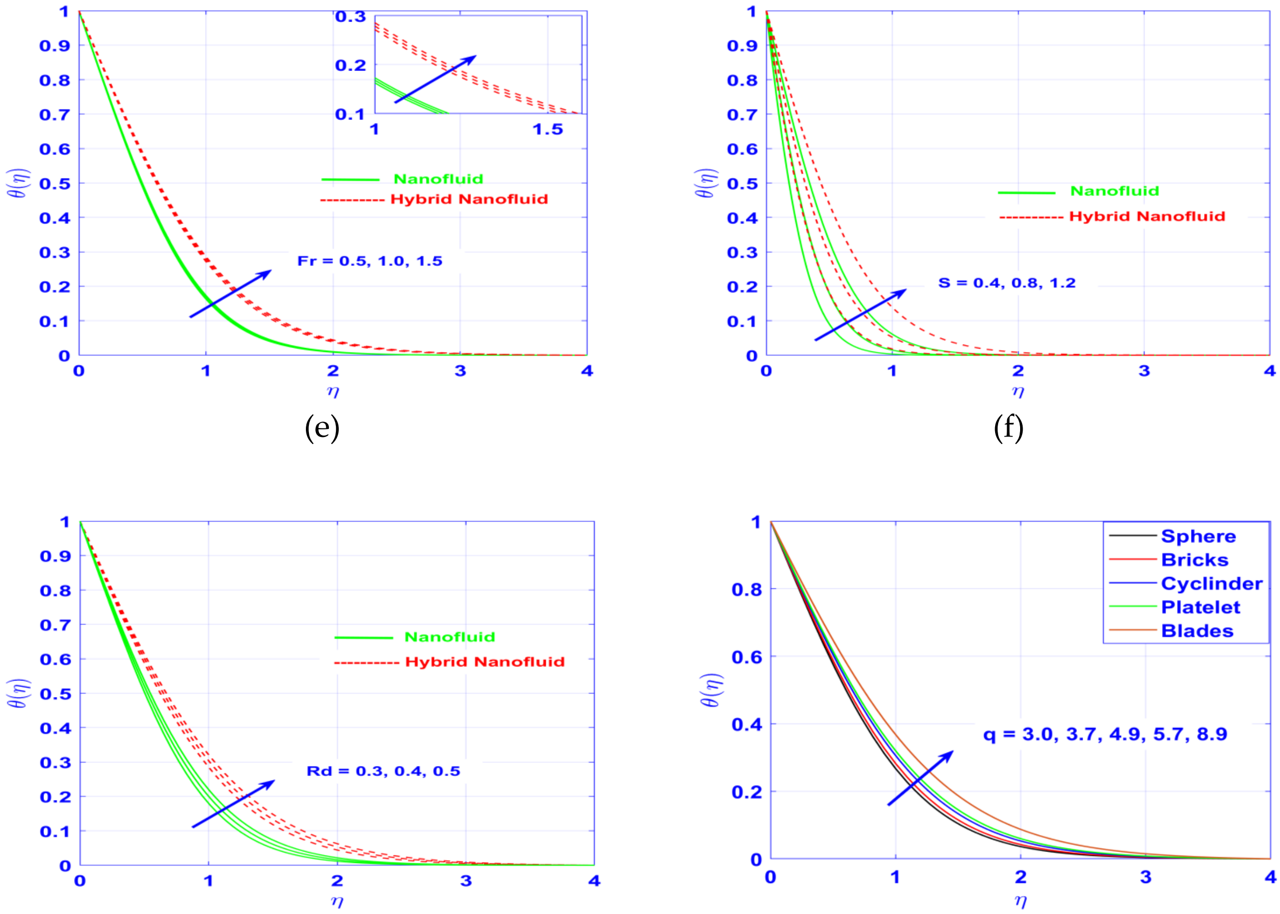

(g) (h)

Figure 4(a-h). Effect of $n, We, M, \lambda, Fr, S, Rd,$ and q on $\theta($

Table 1. Thermo-physical characteristics [31].

Physical Attribute	H_2O	$Al_2O_3(\phi_2)$	$SiO_2(\phi_1)$
$\kappa\ (W.m^{-1}.k^{-1})$	0.613	40.0	1.40
$\rho(kg.m^{-3}.)$	997.1	3970	2200
$Cp\ (J.kg^{-1}.k^{-1})$	4179	765	703

Table 2. Computed values of the friction factors$f''(0)$ *and* $g'(0)$.

λ	Nazar et al. [35]		Farooq et al. [36]		Current results	
	$f''(0)$	$g'(0)$	$f''(0)$	$g'(0)$	$f''(0)$	$g'(0)$
0.0	-1.0000	0.0000	-1.0000	0.0000	-1.0004	0.0000
0.5	-1.1384	-0.5128	-1.1384	-0.5128	-1.1374	-0.5151
1.0	-1.3250	-0.8371	-1.3250	-0.8371	-1.3255	-0.8368
2.0	-1.6523	-1.2873	-1.6523	-1.2873	-1.6523	-1.2873

Table 4. Calculated values of friction factors along the coordinate axis for both (SiO_2 / H_2O) and (SiO_2: Al_2O_3/H_2O).

λ	M	We	n	Fr	S	Po	$Re_x^{0.5}Cf_x SiO_2 / H_2O$	$Re_x^{0.5}Cf_x$ $SiO_2: Al_2O_3/H_2O$	$Re_x^{0.5}Cf_y$ SiO_2 / H_2O	$Re_x^{0.5}Cf_y$ $SiO_2: Al_2O_3/H_2O$
0.5	1.0	0.2	0.1	0.20	0.1	0.1	-1.4134	-1.1844	-0.3178	-0.2440
1.0							-1.5111	-1.2561	-0.5878	-0.4564
1.5							-1.6247	-1.3424	-0.8114	-0.6350
	2.0						-1.6696	-1.4222	-0.2593	-0.1957
	2.5						-1.7875	-1.5304	-0.2396	-0.1800
	3.0						-1.8995	-1.6328	-0.2236	-0.1674
		0.1					-1.3586	-1.1359	-0.3130	-0.2405
		0.2					-1.3763	-1.1516	-0.3146	-0.2417
		0.3					-1.3946	-1.1677	-0.3162	-0.2428
			0.2				-1.2564	-1.0532	-0.2798	-0.2148
			0.4				-1.2125	-1.0195	-0.2615	-0.2006
			0.6				-1.2435	-1.0858	-0.2175	-0.1656
				0.5			-1.4100	-1.1833	-0.3102	-0.2380
				1.0			-1.4920	-1.2586	-0.3059	-0.2342
				1.5			-1.5700	-1.3299	-0.3020	-0.2308
					0.2		-1.4146	-1.1830	-0.3117	-0.2395
					0.4		-1.5328	-1.2825	-0.3075	-0.2362
					0.6		-1.6593	-0.2315	-0.3013	-0.2315
						0.1	-1.4938	-1.2363	-0.3853	-0.30397
						0.3	-1.5437	-1.2729	-0.36947	-0.2929
						0.5	-1.5930	-1.3091	-0.3552	-0.2827

Table 5. Calculated values of heat transfer rate ($\mathrm{Re}_x^{-0.5}Nu_x$) for both (SiO_2 / H_2O) and (SiO_2: Al_2O_3/H_2O).

λ	M	We	n	Rd	S	q	Fr	$\mathrm{Re}_x^{-0.5}Nu_x$ SiO_2 / H_2O	$\mathrm{Re}_x^{-0.5}Nu_x$ $SiO_2: Al_2O_3/H_2O$
0.50	1.0	0.20	0.10	0.30	0.1	3.0	0.20	1.8636	2.1664
1.00								1.8026	2.0915
1.50								1.7332	2.0054
	2.00							1.7902	2.0590
	2.50							1.7571	2.0123
	3.00							1.7265	1.9698
		0.10						1.8704	2.1760
		0.20						1.8682	2.1728
		0.30						1.8659	2.1697
			0.20					1.7987	2.0810
			0.40					1.7486	2.0156
			0.60					1.5833	1.8028
				0.40				1.8379	2.0814
				0.80				1.8084	1.9687
				1.20				1.8053	1.9142
					0.20			2.2594	2.6298

					0.40			3.0877	3.5931
					0.60			3.9655	4.6111
						3.00		1.8704	2.1760
						3.70		1.8730	2.2833
						4.90		1.8760	2.4607
							0.50	1.8594	2.1603
							1.00	1.8421	2.1361
							1.50	1.8260	2.1137

7 | CONCLUSION

This study aims to investigate the enhancement in heat transfer and mass transfer rates of magnetized rotating tangent hyperbolic hybrid nanofluid over a three-dimensional stretching sheet with motile micro-organisms. The flow phenomena have been stated in the PDEs form. Utilizing the similarity variable to convert PDEs into ODEs. These ODEs are numerically solved via the shooting method bvp4c with the MATLAB package. Some important key points that are found are described below.

- It is seen that the distribution of fluid velocity along $x-component$are is reducing, but the profile of fluid velocity along $y-component$are is boosting versus the greater values of $M, \lambda, We, n, Po, Fr$ and S.
- Temperature distribution is upgraded when M, λ, Rd, q, and Svalues are increased.
- The distribution of concentration is boosted with varying values of Nt.
- Concentration distribution is reducing when boosting the values of $Nb\ and\ Le$.
- Motile micro-organism distribution shows a negative change against the large values of Nb, Le, Lb, and Pe.
- Distribution of motile micro-organisms increases while boosting the values of Nt.
- When boosting the values of $M, \lambda, We, n, Po, Fr\ and\ S$then skin fraction coefficient $\left(\boldsymbol{Re_x^{0.5}Cf_x}\right)$are reduced (see Table 4).
- The decrease in the Nusselt number ($\mathrm{Re}_x^{-0.5}\boldsymbol{Nu_x}$) when high values of $\lambda, M, We, n, Fr\ and\ Rd$and grow when high values of $S\ and\ q$(see in Table 5).

Acknowledgment: We are thankful to the editors and anonymous reviewers for their constructive suggestions.

Author Contributions: Conceptualization, M.U.F. and A.M.; methodology, M.U.F., A.M., and F.M.N; software, A.M. and F.M.N.; validation, M.U.F. and A.M.; writing, original draft preparation, M.U.F. and A.M.; writing, review and editing, M.F. and F.S., and S.M. All authors agreed to the manuscript.

Declaration of Conflicting Interest: The author(s) declared no potential conflicts of interest with respect to the research, authorship, and/or publication of this article.

Funding: The author(s) received no financial support for the research, authorship, and/or publication of this article.

Data Availability Statement: Data that supports the findings of this study are available on request from the corresponding author.

Plagiarism Statement: This article was scanned by the plagiarism program. No plagiarism was detected.

REFERENCES

[1] S. U. S. Choi, "Enhancing Thermal Conductivity of Fluids With Nanoparticles," in *Developments and Applications of Non-Newtonian Flows*, San Francisco, California, USA: American Society of Mechanical Engineers, Nov. 1995, pp. 99–105. doi: 10.1115/IMECE1995-0926.

[2] M. Shekaramiz, S. Fathi, H. A. Ataabadi, H. Kazemi-Varnamkhasti, and D. Toghraie, "MHD nanofluid free convection inside the wavy triangular cavity considering periodic temperature boundary condition and velocity slip mechanisms," *Int. J. Therm. Sci.*, vol. 170, p. 107179, Dec. 2021, doi: 10.1016/j.ijthermalsci.2021.107179.

[3] C. Y. Wang, "The three-dimensional flow due to a stretching flat surface," *Phys. Fluids*, vol. 27, no. 8, pp. 1915–1917, Aug. 1984, doi: 10.1063/1.864868.

[4] S. Nadeem and C. Lee, "Boundary layer flow of nanofluid over an exponentially stretching surface," *Nanoscale Res. Lett.*, vol. 7, no. 1, p. 94, Dec. 2012, doi: 10.1186/1556-276X-7-94.

[5] T. Hayat, M. Rashid, M. Imtiaz, and A. Alsaedi, "Magnetohydrodynamic (MHD) stretched flow of nanofluid with power-law velocity and chemical reaction," *AIP Adv.*, vol. 5, no. 11, p. 117121, Nov. 2015, doi: 10.1063/1.4935649.

[6] S. Qayyum, T. Hayat, A. Alsaedi, and B. Ahmad, "Magnetohydrodynamic (MHD) nonlinear convective flow of Jeffrey nanofluid over a nonlinear stretching surface with variable thickness and chemical reaction," *Int. J. Mech. Sci.*, vol. 134, pp. 306–314, Dec. 2017, doi: 10.1016/j.ijmecsci.2017.10.012.

[7] W. A. Khan, M. Ali, M. Shahzad, F. Sultan, M. Irfan, and Z. Asghar, "A note on activation energy and magnetic dipole aspects for Cross nanofluid subjected to cylindrical surface," *Appl. Nanosci.*, vol. 10, no. 8, pp. 3235–3244, Aug. 2020, doi: 10.1007/s13204-019-01220-0.

[8] L. Th. Benos and I. E. Sarris, "The interfacial nanolayer role on magnetohydrodynamic natural convection of an Al_2O_3 -water nanofluid," *Heat Transf. Eng.*, vol. 42, no. 2, pp. 89–105, Jan. 2021, doi: 10.1080/01457632.2019.1692487.

[9] M. Amjad, M. N. Khan, K. Ahmed, I. Ahmed, T. Akbar, and S. M. Eldin, "Magnetohydrodynamics tangent hyperbolic nanofluid flow over an exponentially stretching sheet: Numerical investigation," *Case Stud. Therm. Eng.*, vol. 45, p. 102900, May 2023, doi: 10.1016/j.csite.2023.102900.

[10] T. S. Kumar, "Hybrid nanofluid slip flow and heat transfer over a stretching surface," *Partial Differ. Equ. Appl. Math.*, vol. 4, p. 100070, Dec. 2021, doi: 10.1016/j.padiff.2021.100070.

[11] F. Mabood and A. T. Akinshilo, "Stability analysis and heat transfer of hybrid Cu-Al2O3/H2O nanofluids transport over a stretching surface," *Int. Commun. Heat Mass Transf.*, vol. 123, p. 105215, Apr. 2021, doi: 10.1016/j.icheatmasstransfer.2021.105215.

[12] S. M. Mousavi, M. N. Rostami, M. Yousefi, S. Dinarvand, I. Pop, and M. A. Sheremet, "Dual solutions for Casson hybrid nanofluid flow due to a stretching/shrinking sheet: A new combination of theoretical and experimental models," *Chin. J. Phys.*, vol. 71, pp. 574–588, Jun. 2021, doi: 10.1016/j.cjph.2021.04.004.

[13] T. A. Yusuf, F. Mabood, W. A. Khan, and J. A. Gbadeyan, "Irreversibility analysis of Cu-TiO2-H2O hybrid-nanofluid impinging on a 3-D stretching sheet in a porous medium with nonlinear radiation: Darcy-Forchhiemer's model," *Alex. Eng. J.*, vol. 59, no. 6, pp. 5247–5261, Dec. 2020, doi: 10.1016/j.aej.2020.09.053.

[14] H. A. Ogunseye, Y. O. Tijani, and P. Sibanda, "Entropy generation in an unsteady Eyring-Powell hybrid nanofluid flow over a permeable surface: A Lie group analysis," *Heat Transf.*, vol. 49, no. 6, pp. 3374–3390, Sep. 2020, doi: 10.1002/htj.21778.

[15] L. A. Lund, Z. Omar, J. Raza, and I. Khan, "Magnetohydrodynamic flow of Cu–Fe3O4/H2O hybrid nanofluid with effect of viscous dissipation: dual similarity solutions," *J. Therm. Anal. Calorim.*, vol. 143, no. 2, pp. 915–927, Jan. 2021, doi: 10.1007/s10973-020-09602-1.

[16] B. Ali *et al.*, "Variable Viscosity Effects on Unsteady MHD an Axisymmetric Nanofluid Flow over a Stretching Surface with Thermo-Diffusion: FEM Approach," *Symmetry*, vol. 12, no. 2, p. 234, Feb. 2020, doi: 10.3390/sym12020234.

[17] Z. Abbas *et al.*, "MHD Boundary Layer Flow and Heat Transfer of Nano fluid over a Vertical Stretching Sheet in the Presence of a Heat Source," *Sci. Inq. Rev.*, vol. 3, no. 4, pp. 60–73, Dec. 2019, doi: 10.32350/sir.34.05.

[18] M. R. Eid and F. Mabood, "Entropy analysis of a hydromagnetic micropolar dusty carbon NTs-kerosene nanofluid with heat generation: Darcy–Forchheimer scheme," *J. Therm. Anal. Calorim.*, vol. 143, no. 3, pp. 2419–2436, Feb. 2021, doi: 10.1007/s10973-020-09928-w.

[19] F. Ahmad, S. Abdal, H. Ayed, S. Hussain, S. Salim, and A. O. Almatroud, "The improved thermal efficiency of Maxwell hybrid nanofluid comprising of graphene oxide plus silver / kerosene oil over stretching sheet," *Case Stud. Therm. Eng.*, vol. 27, p. 101257, Oct. 2021, doi: 10.1016/j.csite.2021.101257.

[20] W. Jamshed, K. S. Nisar, S. S. P. M. Isa, S. Batool, A.-H. Abdel-Aty, and M. Zakarya, "Computational case study on tangent hyperbolic hybrid nanofluid flow: Single phase thermal investigation," *Case Stud. Therm. Eng.*, vol. 27, p. 101246, Oct. 2021, doi: 10.1016/j.csite.2021.101246.

[21] M. N. Tamanna, M. Ferdows, G. Lorenzini, M. D. Shamshuddin, and M. Usman, "Numerical Investigation of Heat Transfer Enhancement on Tangent Hyperbolic Fluid over a Stretching Sheet with an Inclined Magnetic Field Filled with Hybrid Nanofluids," *J. Eng. Thermophys.*, vol. 33, no. 1, pp. 55–72, Mar. 2024, doi: 10.1134/S1810232824010065.

[22] M. Nadeem, I. Siddique, Z. Riaz, B. M. Makhdoum, R. M. Zulqarnain, and M. Sallah, "Numerical study of unsteady tangent hyperbolic fuzzy hybrid nanofluid over an exponentially stretching surface," *Sci. Rep.*, vol. 13, no. 1, p. 15551, Sep. 2023, doi: 10.1038/s41598-023-32374-1.

[23] Zaileha Md Ali *et al.*, "Hyperbolic Tangent Fluid Model for Stagnation Flow of Hybrid Nanofluid Over a Stretching Sheet," *J. Adv. Res. Fluid Mech. Therm. Sci.*, vol. 107, no. 1, pp. 87–101, Jul. 2023, doi: 10.37934/arfmts.107.1.87101.

[24] A. Abbas, M. Ashraf, and A. J. Chamkha, "Combined effects of thermal radiation and thermophoretic motion on mixed convection boundary layer flow," *Alex. Eng. J.*, vol. 60, no. 3, pp. 3243–3252, Jun. 2021, doi: 10.1016/j.aej.2021.01.038.

[25] S. Lie, *Sophus Lie's 1884 Differential Invariant Paper, Vol. 3*. Brookline, MA: Math Science Press, 1976.

[26] A. A. Avramenko, S. G. Kobzar, I. V. Shevchuk, A. V. Kuznetsov, and L. T. Iwanisov, "Symmetry of turbulent boundary-layer flows: Investigation of different eddy viscosity models," *Acta Mech.*, vol. 151, no. 1–2, pp. 1–14, Mar. 2001, doi: 10.1007/BF01272521.

[27] A. Rashid, M. Ayaz, S. Islam, A. Saeed, P. Kumam, and P. Suttiarporn, "Theoretical analysis of the MHD flow of a tangent hyperbolic hybrid nanofluid over a stretching sheet with convective conditions: A nonlinear thermal radiation case," *South Afr. J. Chem. Eng.*, vol. 42, pp. 255–269, Oct. 2022, doi: 10.1016/j.sajce.2022.09.005.

[28] V. J. Prajapati and R. Meher, "Analysis of MHD tangent hyperbolic hybrid nanofluid flow with different base fluids over a porous stretched sheet," *J. Taibah Univ. Sci.*, vol. 18, no. 1, p. 2300851, Dec. 2024, doi: 10.1080/16583655.2023.2300851.

[29] R. K. Tiwari and M. K. Das, "Heat transfer augmentation in a two-sided lid-driven differentially heated square cavity utilizing nanofluids," *Int. J. Heat Mass Transf.*, vol. 50, no. 9–10, pp. 2002–2018, May 2007, doi: 10.1016/j.ijheatmasstransfer.2006.09.034.

[30] T. Hayat, F. Haider, T. Muhammad, and A. Alsaedi, "Three-dimensional rotating flow of carbon nanotubes with Darcy-Forchheimer porous medium," *PLOS ONE*, vol. 12, no. 7, p. e0179576, Jul. 2017, doi: 10.1371/journal.pone.0179576.

[31] P. Nanda, N. Sandeep, C. Sulochana, and G. P. Ashwinkumar, "Enhanced heat transmission in methanol-based AA7072/AA7075 tangent hyperbolic hybrid nanofluid flow along a nonlinear expandable surface," *Numer. Heat Transf. Part Appl.*, vol. 83, no. 7, pp. 711–725, Apr. 2023, doi: 10.1080/10407782.2022.2157916.

[32] S. A. A. Shah and A. U. Awan, "Significance of magnetized Darcy-Forchheimer stratified rotating Williamson hybrid nanofluid flow: A case of 3D sheet," *Int. Commun. Heat Mass Transf.*, vol. 136, p. 106214, Jul. 2022, doi: 10.1016/j.icheatmasstransfer.2022.106214.

[33] N. S. Anuar, N. Bachok, and I. Pop, "Radiative hybrid nanofluid flow past a rotating permeable stretching/shrinking sheet," *Int. J. Numer. Methods Heat Fluid Flow*, vol. 31, no. 3, pp. 914–932, Mar. 2021, doi: 10.1108/HFF-03-2020-0149.

[34] S. P. A. Devi and S. S. U. Devi, "Numerical Investigation of Hydromagnetic Hybrid $Cu - Al_2O_3$ /Water Nanofluid Flow over a Permeable Stretching Sheet with Suction," *Int. J. Nonlinear Sci. Numer. Simul.*, vol. 17, no. 5, pp. 249–257, Aug. 2016, doi: 10.1515/ijnsns-2016-0037.